HHS Public Access

Author manuscript

Neuron. Author manuscript; available in PMC 2020 January 16.

Published in final edited form as:

Neuron. 2019 January 16; 101(2): 224–231.e5. doi:10.1016/j.neuron.2018.11.032.

Axoglial adhesion by Cadm4 regulates CNS myelination

Nimrod Elazar[1], **Anya Vainshtein**[1], **Neev Golan**[1], **Bharath Vijayaragavan**[1], **Nicole Schaeren-Wiemers**[2], **Yael Eshed-Eisenbach**[1], and **Elior Peles**[1,*]

[1.]Department of Molecular Cell Biology, The Weizmann Institute of Science, Rehovot 76100, Israel [2.]Department of Biomedicine, University Hospital Basel, Basel CH- 4031, Switzerland

SUMMARY

The initiation of axoglial contact is considered a prerequisite for myelination, yet the role cell adhesion molecules (CAMs) play in mediating such interactions remains unclear. To examine the function of axoglial CAMs, we tested whether enhanced CAM-mediated adhesion between OLs and neurons could affect myelination. Here we show that increased expression of a membrane-bound extracellular domain of Cadm4 (Cadm4dCT) in cultured oligodendrocytes results in the production of numerous axoglial contact sites that fail to elongate and generate mature myelin. Transgenic mice expressing Cadm4dCT were hypomyelinated and exhibit multiple myelin abnormalities including myelination of neuronal somata. These abnormalities depend on specific neuron-glial interaction as they were not observed when these OLs were cultured alone, on nanofibers, or on neurons isolated from mice lacking the axonal receptors of Cadm4. Our results demonstrate that tightly regulated axon-glia adhesion is essential for proper myelin targeting and subsequent membrane wrapping and lateral extension.

eTOC

Elazar et al., demonstrate that myelination requires regulated adhesive interactions between oligodendrocytes and axons. They show that excessive axoglial contact results in mistargeting of oligodendrocytes to neuronal somata, and their inability to form elongated myelin around axons.

INTRODUCTION

Myelination in the central nervous system involves a complex set of intercellular contacts between oligodendrocytes (OLs) and their underlying axons. These interactions are believed

Address correspondence to: Dr. Elior Peles, Department of Molecular Cell Biology, The Weizmann Institute of Science, Rehovot 76100, Phone: (972) 8-934-4561, Fax: (972) 8-934-4195, peles@weizmann.ac.il.

AUTHOR CONTRIBUTIONS

N.M. and E.P. designed the study. N.M. A.V. N.G. B.R. and Y.E.E performed experiments and analyzed data. N.S.W. provided essential reagents, E.P. wrote the paper with input from all authors.

*Lead contact and corresponding author.

DECLARATION OF INTERESTS

The authors declare no competing interests.

to regulate distinct stages of myelinogenesis including target selection, membrane ensheathment, longitudinal extension of the myelin unit, and functional organization of the axonal membrane (Osso and Chan, 2017; Snaidero and Simons, 2017). During development, OLs send multiple exploratory cellular processes that contact numerous axons. Some of these processes are stabilized and develop into myelin internodes while the rest eventually retract (Czopka et al., 2013; Hines et al., 2015). This process may share some similarities with synaptogenesis, where CAMs mediate initial target recognition as well as a second step of stabilization (Almeida and Lyons, 2014). Although OLs express a number of cell adhesion molecules (CAMs) (Marques et al., 2016; Sharma et al., 2015; Zhang et al., 2014), these often have redundant functions, making it difficult to assess their individual roles and the importance of cell adhesion during myelination.

To examine the role of axoglial CAMs in myelination, we tested whether enhanced adhesion between OLs and neurons could affect myelination and in what manner. We chose to express the extracellular domain of Cell adhesion molecule 4 (Cadm4) on the OLs cell surface as this CAM is enriched in myelinating OLs (Marques et al., 2016; Zhang et al., 2014) and is expressed at the onset of myelination (Figure S1). Cadm4 is a member of a small group of CAMs (Cadm1-Cadm4), also known as synaptic cell adhesion molecules (SynCAM) or Nectin like adhesion molecules (Necl), which are characterized by the presence of three immunoglobulin-like domains in their extracellular region (Takai et al., 2008). Cadm4 mediates internodal axoglial adhesion by binding to axonal Cadm2 and Cadm3 in both the peripheral (Maurel et al., 2007; Spiegel et al., 2007) and central (Pellissier et al., 2007; Sharma et al., 2015; and Figure S4A) nervous systems. However, in line with the presence of multiple members of this family in both neurons and myelinating glia and their combinatorial heterophilic binding properties, as well as their redundant function in other systems (Fowler et al., 2017), genetic deletion of individual Cadm genes in mice resulted in only marginal myelination phenotypes (Golan et al., 2013; Park et al., 2008; Zhu et al., 2013). By using a different experimental approach that relies on the expression of the extracellular domain of Cadm4 in OLs we reveal a critical role for cell adhesion in myelin targeting, membrane wrapping and lateral extension of the myelin sheath.

RESULTS

Expression of Cadm4's extracellular domain in OLs interferes with myelination.

To assess the contribution of Cadm-mediated axon-oligodendrocyte adhesion in myelination, we infected rat oligodendrocyte precursor cells (OPCs) co-cultured with sensory neurons with a retroviral vector that directs the expression of only the extracellular and transmembrane domains of Cadm4 (Cadm4dCT) in a tetracycline-inducible manner (STAR methods). The construct also included a short myc-tag that enabled the detection of Cadm4dCT-expressing OLs. We reasoned that while such a protein would still be able to mediate cell-cell adhesion, it would be devoid of intracellular signaling capabilities. Induction of Cadm4dCT expression by doxycycline resulted in a pronounced morphological abnormality of myelinating OLs (Figure 1A-B). Immunolabeling for MBP revealed that in contrast to the untreated cells, which produced a limited number (9±4) of long myelin internodes (average segment length of 48±26 μm), Cadm4dCT expressing OLs formed many

(100±30) short segments (average segment length of 9±14 μm) (Figure 1C-D). Intriguingly, these short oligodendroglial segments were predominantly aligned with axons (Figure S2A), indicating that Cadm4dCT OLs may form excessive axon-glia contact.

To further examine the role of Cadm4-mediated adhesion *in vivo,* we have analyzed transgenic mice in which Cadm4dCT was placed under the *MBP* promoter *(Tg(mbp-Cadm4dCT);* Golan et al., 2013). These mice expressed the Cadm4dCT transgene in OLs throughout the white matter (Figure S2B). The expression of Cadm4dCT also caused a slight reduction if the expression of the endogenous Cadm4 (data not shown). Luxol fast blue (LFB) staining of sagittal brain sections showed that compared to wild type mice, *Tg(mbp-Cadm4dCT)* exhibited pronounced hypomyelination in different brain regions, including the corpus callosum, cerebellar white matter and spinal cord (Figure 1E-G). In the cerebellum, hypomyelination was already detected at P12, and was clearly observed at P21 and P90 (Figure S2E). As detected by immunolabeling of cerebellar and cortical sections with antibodies to MBP and PLP, *Tg(mbp-Cadm4dCT)* myelin appeared short *(WT,* 18±12 μm and *Cadm4dCT,* 6±6 μm) and patchy (Figure 1H-J), resembling myelinating OLs expressing Cadm4dCT in culture (Figure 1A). In accordance with the aberrant myelination elicited by Cadm4dCT in the cortex, we noted a reduction in the number of Caspr-labeled paranodal junctions *(Cadm4dCT* 60±18 vs 198±40 in wild type) (Figure 1K-L). Immunolabeling of cerebellar sections using the CC1 antibody demonstrated a comparable number of myelinating OLs in *Tg(mbp-Cadm4dCT)* (94±25) and wild type mice (80±23) (Figures S2C-D), indicating that Cadm4dCT did not affect the number of OLs. Similar results were observed in the optic nerve *(WT,* 84±15 vs 95±22 in *Cadm4dCT)* (Figures S3D,E).

Tg(mbp-Cadm4dCT) mice exhibit diverse and severe myelin abnormalities.

Transmission electron microscopy (EM) analysis of the corpus callosum of three-month-old *Tg(mbp-Cadm4dCT)* mice showed a mixed hypo- and hyper-myelination phenotype (Figure 2A-B). Compared to wild type tissue, only one-third of the axons were myelinated (Figure 2C), and many axons were surrounded by abnormally thick myelin (*g* ratio <0.65) (Figure 2B, D-F). In addition, *Tg(mbp-Cadm4dCT)* corpus callosum and spinal cord displayed a range of myelin abnormalities including extended myelin outfolds, myelin splitting, and vacuolization (Figure 2G-H and I-M). Vacuolization and myelin loss was more pronounced in the spinal cord and the cerebellum (Figure S2E and data not shown) than in the corpus callosum, possibly resulting from the difference in axonal diameter in these tissues. More than 50% of the myelin profiles in the spinal cord and corpus callosum of *Tg(mbp-Cadm4dCT)* were abnormal (Figure 2I). Longitudinal sections of *Tg(mbp-Cadm4dCT)* optic nerve showed no apparent hypomyelination but presence of a remarkably short (10.5μm) internode (Figure S3A). As expected, the reduction in internodal length in the optic nerve was also reflected by an increase in the number of βIV spectrin-labeled nodes of Ranvier in the mutant (3200±270 in wild type vs 3803±560 in *Cadm4dCT),* but not in the number of CC1 labeled OLs (Figure S3B-E). The increase in nodal density in the optic nerve was in contrast to the observed reduction in the number of paranodes in the cortex (Figure 1L). This observation reflects the inherent difference between white and gray matter myelination and the fact that the former exhibit larger density of OLs and available axons, which allow the

formation of higher number of axoglial contact sites in the transgene. Notably, in peripheral nerves we also found an increase in nodal density (Figure S3F-G; mean of 58±12 in wild type vs 144±27 in Cadm4dCT), and a marked decrease in internodal length (Figure S3H; e.g., 1104 pm in wild type vs 202±28 pm in Cadm4dCT in the presented example).

Cadm4dCT oligodendrocytes produce numerous contact sites but fail to elongate and generate mature myelin internodes.

To further examine the phenotype of OLs expressing Cadm4dCT, we co-cultured OPCs isolated from wild type and *Tg(mbp-Cadm4dCT)* brains with sensory DRG neurons and traced the cellular processes of individual cells. We found that while each wild type oligodendrocyte formed a restricted number (average of 24±17 per cell) of MBP-labeled myelin segments, OLs expressing Cadm4dCT formed many more (average of 152±55 per cell) MBP-positive segments around axons (Figure 3A-E). Cadm4dCT myelin segments were shorter than the ones formed by wild type cells (average of 6±6 μm Cadm4dCT vs 30±25 μm wild type), with only less than 20% of the segments being longer than 10 μm, compare to >80% in the wild type (Figure 3E). These segments were often formed by a thin cellular process that originated from a proximal short myelin segment that failed to elongate (Figure 3C). As expected, the increase number of short myelin segments resulted in increased number of Caspr clusters that were associated with individual OLs (Figure 3G-F).

Cadm4dCT oligodendrocytes myelinate neuronal cell bodies.

Recent studies suggest that the balance between positive and negative signals regulate myelin targeting (Almeida et al., 2018; Osso and Chan, 2017; Redmond et al., 2016). To determine whether the excessive oligodendrocyte adhesion conferred by Cadm4dCT could change myelin targeting, we examined whether *Tg(mbp-Cadm4dCT)* OLs myelinate non-axonal structures. We concentrated our attention on neuronal cell bodies since they are not usually myelinated but express the neuronal receptors for Cadm4 as inferred by binding of the extracellular domain of Cadm4 (Figure S4C). As depicted in Figure 3H, we observed neuronal cell body ensheathment in myelinating spinal cord culture prepared from a double transgenic mouse expressing both Cadm4dCT and MAG-GFP (Erb et al., 2006). Given that early differentiating OLs make transient contact with neuronal cell bodies (Almeida et al., 2018 and Supplement Figure S3J-K), we searched for cell body myelination in adult (P90) mouse brains by labeling for MBP. We detected extensive ensheathment of neuronal cell bodies in the cerebellum of *Tg(mbp-Cadm4dCT)* but not in wild type mice (Figure 3I-J). Furthermore, in marked contrast to wild type mice, we noted the ensheathment of neuronal cell bodies in other brain areas such as the olfactory bulb (Figure S3I) and hippocampus (data not shown). In agreement, using transmission electron microscopy we detected the presence of multiple myelin layers around cell bodies in the cerebellum of *Tg(mbp-Cadm4dCT)* mice (Figure 3K-O). These observations, along with the multiple MBP segments observed in association with Cadm4dCT-expressing OLs, suggest that early OL-neurons interactions are prematurely stabilized in cells expressing Cadm4dCT.

Myelin abnormalities result from specific Cadm4-mediated neuron-glia adhesion.

Our results indicate that adhesive interactions between oligodendrocyte processes and axons regulate myelin targeting, as well as membrane wrapping and longitudinal extension that are

required for the formation of mature myelin internodes. In *Tg(mbp-Cadm4dCT)* mice, expression of the extracellular domain of Cadm4 in OLs results in excessive adhesion, leading to both mistargeting (i.e., wrapping of neuronal cell bodies), and myelination failure. We reasoned that if the abnormalities detected in *Tg(mbp-Cadm4dCT)* mice are indeed dependent upon neuron-glia adhesion mediated by Cadm4, they would not be detected if these OLs were either grown alone, or on nanofibers, which lack specific axonal adhesive molecules but enable membrane ensheathment (Bechler et al., 2015; Lee et al., 2012). Indeed, we found that when grown in the absence of neurons, the morphology of OLs expressing Cadm4dCT as assessed by MBP immunoreactivity, was indistinguishable from wild type cells *(WT* 12±6.8 mm^2 vs 12±9.8 m^2 in *Cadm4dCT)* (Figure 4A-B). We next isolated OPCs from wild type and *Tg(mbp-Cadm4dCT)* mice and cultured them for 10 days on either neurons or polystyrene nanofibers before labeling with antibodies to MBP or to opalin, which labels the oligodendrocyte cell soma, processes and myelinated internodes (Golan et al., 2008). We found that while Cadm4dCT OLs were clearly distinct from wild type cells when grown in the presence of neurons, they displayed identical morphology to wild type OLs when grown on nanofibers (Figure 4C). As an additional approach, we infected rat OPCs with a retroviral vector that enables the induction of Cadm4dCT expression by doxycycline prior to placing the cells on nanofibers (i.e prior to MBP expression). Similar to the results obtained with *Tg(mbp-Cadm4dCT)* isolated cells, we found no difference in the morphology of doxycycline-treated or non-treated OLs (Figure 4D). To further determine if the phenotype of OLs expressing Cadm4dCT is due to increased neuron-glia adhesion, we isolated OPCs from *Tg(mbp-Cadm4dCT)* mice and cultured them with neurons isolated from either wild type or mice lacking both Cadm2 and Cadm3, which serve as the axonal receptors of Cadm4 (Figure S4A-B and Maurel et al., 2007; Spiegel et al., 2007). We found that Cadm4dCT OLs grown on $Cadm2^{-/-}/Cadm3^{-/-}$ neurons displayed fewer MBP-labeled processes associated with axons (average of 31 ±9 per cell) compared to those grown on wild type neurons (average of 157±41 per cell) (Figure 4E-F). This phenotypic attenuation was also accompanied by an increase in process length, with only less than 15% being smaller than 5 μm when Cadm4dCT oligodendrocyte were grown on $Cadm2^{-/-}/Cadm3^{-/-}$ neurons, compared to >55% when they were grown on wild type neurons (Figure 4G).

DISCUSSION

Our results reveal an important role for axoglial cell adhesion molecules in CNS myelination by regulating target selection, myelin wrapping and internodal extension. This conclusion is based on the following findings: ***i.*** Expression of the extracellular region of Cadm4 in OLs grown with wild type neurons *in vitro* resulted in the formation of excess axonal contacts which failed to generate myelin internodes. ***ii.*** This phenotype could be rescued by removal of the neuronal Cadm4 receptors (i.e., Cadm2 and Cadm3), and was not detected when Cadm4dCT expressing OLs were either cultured alone or on nanofibers. ***iii.*** Transgenic mice expressing *Cadm4dCT* under the MBP promoter display severe hypomyelination as well as additional myelin abnormalities in both gray and white matter. ***iv.*** OLs expressing Cadm4dCT are mistargeted and ensheath neuronal cell bodies.

The inability of Cadm4dCT to form mature elongated internodes *in vitro,* along with the presence of the unusually short internodes detected in *Tg(mbp-Cadm4dCT)* optic nerve, indicate that cell adhesion plays an important role in the lateral extension of the forming myelin segment. Given the coupling of membrane wrapping with internodal extension (Snaidero et al., 2014), the lateral extension abnormality may be secondary to a membrane wrapping defect. During myelination, the leading edge of the myelin sheath grows around the axon while displacing the previously deposited membrane (Snaidero et al. 2014), a process that would be disrupted by excessive axoglial adhesion. In addition, Cadm4dCT OLs established numerous short MBP-labeled myelin segments on adjacent axons that were often linked by a single cellular process. These reflect the inability of the mutant OLs to retract the initial contacts made during the early exploratory stage of myelination (Czopka et al., 2013; Watkins et al., 2008). In line with this notion, time-lapse microscopy of myelinating spinal cord cultures made from *Tg(mag-GFP)* and *Tg(mag-GFP/mbp-Cadm4dCT)* mice showed that while wild type OLs sent processes that dynamically attached, retracted and myelinated axons, Cadm4dCT OLs attached axons but remained relatively static (data not shown).

Excessive axoglial contact results in the stabilization of early and otherwise transient axoglial interactions as evident by the ensheathment of neuronal somas. In agreement with the observations Almeida et al. made *in vivo* in the zebrafish (Almeida et al., 2018), we found that during early stages of myelination in cultures (DIV3), 27% of O4-positive cell processes attached to neuronal cell bodies, but these processes retracted with further differentiation and myelination and reached only 2.5% at DIV11 (Figure S3J-K). In Cadm4dCT OLs these early transient contacts persist, leading to ectopic ensheathment and myelination of neuronal cell bodies both *in vitro* and *in vivo.* The avoidance of OLs from neuronal cell bodies is controlled by inhibitory signals such as JAM2, an immunoglobulin CAM present at the somatodendritic compartment (Redmond et al., 2016). It is also regulated by positive axonal signals, as evident by the recent observation that cell body myelination occurs when the number of OLs exceeds axonal availability (Almeida et al., 2018). In this case, myelination of non-axonal structures is enabled by the lack of sufficient positive axonal signals. Our results show that myelin targeting is regulated by oligodendrocyte-neuron adhesion, and that neuronal cell body myelination could also occur as a result of an increase in adhesion mediated by axoglial CAMs in non-axonal structures.

In addition to neuronal cell body myelination, Tg(mbp-*Cadm4dCT*) mice exhibit several other myelin abnormalities including short and aberrant myelin segments, intramyelinic swelling and myelin outfoldings, all of which demonstrate that regulated axon-glia adhesion is required to form and maintain the intricate myelin unit. Tg(mbp-*Cadm4dCT*) mice also display a mixed hypo- and hyper-myelination phenotype in the corpus callosum. While hypomyelination is in line with the notion that Cadm4dCT expression leads to excessive adhesion and unregulated cell-cell contact, the presence of hypermyelination is less clear and may reflect a requirement for the cytoplasmic domain of Cadm4 in mediating a negative feedback signal from axons undergoing myelination back to the overlying OLs. In support of this idea, expression of the cytoplasmic domain of Cadm4 in Schwann cells inhibits myelination (Spiegel et al., 2007).

In summary, we demonstrate that enhanced oligodendrocyte-neuron adhesion elicited by the expression of the extracellular domain of Cadm4 on the OLs surface results in premature stabilization of axon-glial contacts, a defect in target recognition, membrane wrapping and lateral extension. Our results indicate that intercellular interactions mediated by cell adhesion molecules are important during several stages of CNS myelination. They also reveal that axon-glia adhesion should be tightly regulated during myelination, possibly by post translational modification (Fogel et al., 2010; Galuska et al., 2010) and proteolytic processing-mediated ectodomain shedding (Tanabe et al., 2008) of the underlying adhesion proteins.

STAR METHODS

Contact and Reagent Resource Sharing

Further information and requests for resources and reagents should be directed to and will be fulfilled by the Lead Contact, Elior Peles (peles@weizmann.ac.il).

Experimental Model and Subject Details

Mouse models—Post neonatal day P0-P21 and adult P60 and P90 mice were used in this study as indicated. All transgenic and knock out mice were kept on a C57BL/6 background (RRID:MGI:5656552,Jackson Laboratory, Bar Harbor, MA). *Tg(mbp-Cadm4dCT), Cadm2*$^{-/-}$, *Camd3*$^{-/-}$, *Camd4*$^{-/-}$ *and CNP-Cre:Rosa26-lacZfloxDTA* mice were previously described (Golan et al., 2013; Brockschnieder et al., 2006). For all experiments, both male and female littermates were randomly assigned to experimental groups. Animals were housed in a temperature-controlled animal room with a 12h light/dark cycle. Water and food were available ad libitum. E13.5 mouse embryos and E15.5 Wistar rat (RGD_13525002) embryos obtained from timely pregnant female, and P0-P2 mouse pups and P5-8 Wistar rat pups, were used for primary cultures. All experiments were performed in compliance with the relevant laws and institutional guidelines and were approved by the Weizmann Institute's Animal Care and Use Committee.

Primary cultures—Co-cultures of OPCs with DRG neurons were generated using DRG neurons isolated from rat or mouse embryos at E15.5 and E13.5, respectively. Embryos were genotyped and pooled irrespective of sex, and DRGs were removed in cold L-15 medium. Tissue was dissociated in 0.25% trypsin, triturated, centrifuged, and re-suspended in NB medium (Neurobasal, B27 supplement, 0.5 mM L-glutamine, and penicillin-streptomycin). For all experiments, pre-cleaned 13mm diameter glass coverslips were placed in 4-well dishes and coated with Matrigel (1 hour at RT) and poly-D-lysine (30 minutes at RT) prior to dissection. Cells were plated at a density of 40,000 cells/13mm coverslips in NB medium and maintained in a humidified incubator at 37°C and 5% CO_2. Cultures were treated with fluorodeoxyuridine at DIV2, 4 and 6 to eliminate non-neuronal cells. Fifty percent of cell media was replaced every third day and OPCs were added on DIV15. OPCs were genotyped from rat or mouse pups aged P5-P8 and P0-P2, respectively. Cortices were isolated in ice-cold L-15 medium and dissociated using 0.25% trypsin (for rat tissue) or syringe (19G followed by 21G for mouse tissue), triturated, centrifuged, and re-suspended in glial plating medium (DMEM containing 10% fetal bovine serum, penicillin-streptomycin for rat glia

and DMEM/F-12 containing 10% fetal bovine serum, 5% horse serum and penicillin-streptomycin) on PDL-coated flasks. Glial cells were maintained in a humidified incubator at 37°C and 5% CO_2, and fifty percent of cell medium was changed every third day. At DIV10 OPCs were isolated by shaking the flasks vigorously, followed by depletion of astrocytes by fast adhesion to culture dishes (10 minutes at 37°C x3) or by negative immunopanning on anti-RAN2 Ab-coated plates. Purified OPCs (200,000/coverslip) were seeded on DRG neuronal cultures and maintained in co-culture medium (DMEM containing B27 and N2 supplements, 5μg/ml N-Acetyl-Cysteine, 5μM forskolin, penicillin-streptomycin). The medium was changed every other day for 9-11 days.

For myelinating spinal cord cultures, spinal cords isolated from genotyped E13.5 mice embryos were transferred to HBSS and dissociated using 0.25% trypsin and 0.1% collagenase. Cells were collected, resuspended in spinal cord plating medium (DMEM containing 25% horse serum, 25% HBSS and 4mM glutamine) and plated (300,000/13mm coverslip) on 0.1% PLL coated coverslips. Three hours post seeding, the medium was changed to differentiation medium (DfM: DMEM containing 0.5% hormone mix i.e. 1 mg/mL apo-transferrin, 20 mM putrescine, 4 μM progesterone, and 6 μM selenium,10 ng/mL biotin and 50 nM hydrocortisone). Insulin (10 μg/mL) was added to the DfM for the first 12-14 days. Medium was changed every other day for 28 days. Cells from at least three independent experiments were analyzed.

For isolated oligodendrocyte cultures, mouse and rat OPCs obtained from glial mixed cultures were seeded on PDL coated coverslips and maintained in Sato medium (DMEM containing B-27 supplement, Glutamax, penicillin-streptomycin, 1% horse serum, sodium pyruvate, 0.34μg/ml T3 and 0.4 μg/ml T4). The medium was changed every other day for 9-11 days. Between 7 to 20 cells from at least three independent experiments were analyzed and subjected to unpaired Student's t-test with two tails. For nanofibers experiments, OPCs were cultured with 700-nm diameter polycaprolactone (PCL) Nanofibers (Nanofiber Solutions, Cat number: 121202) in Sato medium. Cultures were maintained at 37°C, in a humidified incubator (5% CO_2) and medium was changed every other day for 9-11 days. Cells from at least three independent experiments were analyzed.

Method Details

Expression of Cadm4dCT in myelinating co cultures—Expression of Cadm4dCT in cultures was achieved using the Tet-One expression system (Clontech) that allows inducible expression upon addition of doxycycline. pMX-TetOne-Cadm4dCT plasmid was generated by inserting a Myc-tagged Cadm4 cDNA lacking its cytoplasmic tail (Spiegel et al., 2007) into a pMX-TetOne vector (adapted from Clontech Takara). Retroviral particles were produced by transfection of pMX-TetOne-Cadm4dCT into sub-confluent HEK293 Phoenix-ECO packaging cells. Viral supernatant was collected after 72 hours, centrifuged, aliquoted and stored at −80°C. OPCs were infected at DIV3 of mixed glial cultures by adding 5ml viral supernatant to each flask for 48-72 hours. At DIV10, rat OPC's were shaken off, collected and seeded on pre-cultured DRG neurons. OPC-DRG co cultures were maintained in co-culture medium as described above. Induction of expression was obtained by addition of doxycycline (0.5μg/μl) 72 hours post seeding for the duration of the culture

(9-11 days). Cultures were fixed using 4% PFA for 10 min at RT and subsequently analyzed by Immunofluorescence. Between 14 to 20 cells from at least three independent experiments were analyzed and subjected to unpaired Student's t-test with two tails.

Histology and immunofluorescence—At least three mice of each genotype were anaesthetized and perfused with 2% PFA/PBS. Brains and optic nerves were isolated and post-fixed on ice for 30 min. For immunofluorescence, tissues were incubated in 30% sucrose/PBS at 4°C overnight, embedded in OCT and sectioned. 12 μm sections were washed with PBS and blocked with PBS containing 5% normal goat serum, 0.5% Triton X-100, 0.05% sodium azide for 1h at RT. For peripheral nerves, mice were anaesthetized, sciatic nerves were excised and fixed in 4% PFA/PBS for 30 minutes on ice. Nerves were either teased on glass slides or incubated in 30% sucrose/PBS at 4°C overnight and sectioned as above. All samples we re incubated overnight at 4°C with primary antibodies diluted in PBS containing 5% normal goat serum, 0.5% Triton X-100, 0.05% sodium azide, washed three times in PBS, incubated for 1 h with secondary antibodies, washed in PBS and mounted with Fluoromount-G. Immunohistochemistry of paraffin sections (6 μm) was performed following deparaffinization, rehydration (graded ethanol solutions) and antigen retrieval (10mmol/L citrate, pH 6.0, at 95°C for 10-15 minutes). For immunocytoc hemistry, cells from at least three independent experiments were fixed using 4%PFA for 10 min at RT and subsequently washed with PBS and immunolabeled as described above. As detailed in the Key Resource Table, the following primary antibodies were used for immunostaining: rat anti-MBP (1:300), rat anti-PLP (1:20) mouse anti-Myc (1:500), mouse anti-O4 (1:50), rabbit anti-Myc (1:1000), Rat anti-Neurofilament H (1:200), mouse anti-NF (1:2000), mouse anti-CC1 (1:50), rabbit beta 4 spectrin (1:600, gift from Dr. Matt Rasband), Rabbit anti-Opalin (1:500), Rabbit anti-Caspr (1:500). Secondary antibodies coupled to Dylight 405, 488, Cy3, Dylight 647, Cy5, and Cy3 were from Jackson ImmunoResearch.

Fc-fusion binding experiments were performed by incubating cells with medium containing various Fc-fusion proteins pre-incubated with Cy3-conjugated anti-human antibody (Jackson ImmunoResearch). Myelinating spinal cord cultures were incubated with medium containing the respective pre-clustered Fc–fusion protein for 1h at RT washed once and grown for additional 2 hours before fixing.

Luxol Fast Blue (LFB) staining was preformed using the NovaUltra luxsxol fast blue stain kit. Briefly, paraffin embedded brain sections (6 μm) from at least three mice of each genotype were dewaxed followed and rehydrated to 95% ethanol after which sections were incubated in LFB solution (0.1% LFB in 95% ethanol/0.5% acetic acid) overnight at 56°C. Se ctions were then washed in 95% ethanol and ddH2Ofollowed by 0.05% lithium carbonate for 30 seconds, and then with 70% ethanol until the grey matter was colorless and white matter appeared blue. Sections were then rinsed in ddH2O before counterstaining with preheated 0.1% Cresyl Violet acetate solution for 30-40 seconds. Finally, sections were rinsed in ddH2O, dehydrated with 100% ethanol and xylene and mounted with resinous medium.

Image processing and analysis—Images were acquired using an LSM700 confocal microscope (Carl Zeiss), panoramic digital slide scanner (3DHISTECH) or Tecnai Spirit or

T12 transmission electron microscope. For most images, processing included only global change of contras and brightness. For image analysis, images were taken in equivalent spatial distribution; Analyses were performed while blinded to genotype. Tissues and cells stained positively for Myc-tag were regarded as mutant. Figures display representative images. Image analysis was performed using Image J (NIH) and ZEN 2011 (Carl Zeiss) software.

Electron microscopy—Mice were anaesthetized and perfused with a fixative containing 4% PFA, 2.5% glutaraldehyde and 0.1 M cacodylate buffer. Brains and spinal cords were isolated and incubated in the fixative overnight at room temperature and processed as previously described (Yang et al., 2015). Samples were examined using a Tecnai Spirit or T12 transmission electron microscope, equipped with a FEI Eagle camera or a Gatan ES500W Erlangshen camera respectively. EM micrographs were analyzed using computer-assisted Image J (NIH) analysis software, for axon diameter and total outer axon diameter containing myelin. G-ratio was calculated by dividing the measured inner axonal diameter to the measured total outer axonal diameter. At least 1300 axons from three mice of each genotype were analyzed and subjected to unpaired Student's t-test with two tails.

Western Blots—P0-P60 mouse brains were lysed in RIPA buffer (10 mM Tris-Cl pH 8.0, 1mM EDTA,1% Triton X-100, 0.1% sodium deoxycholate, 0.1% SDS,140 mM NaCl, 1 mM PMSF) supplemented with protease inhibitors. Equal amounts of protein were loaded onto a 10% SDS-PAGE gel and transferred to PVDF membrane. Membranes were blotted with antibodies to Cadm4, tubulin, MAG and MBP, reacted with HRP-conjugated secondary antibodies, developed by ECL, and imaged on Bio-Rad ChemiDOCTM.

Quantification and Statistical Analysis

All graphs and statistical tests were carried out using Microsoft Excel, throughout the figures data are presented as the mean ±SEM or average ±SDTV as indicted in figure legends. Statistical analyses were performed using an unpaired Student's t-test with two tails. We considering a difference significant when $p < 0.05$. Throughout the figures, we indicate p values as follows: no significance or 'ns' for $p > 0.05$, or '*' for $p < 0.05$'. For *in vivo* experiments, at lest three aged-matched mice were used. Sample size was not predetermined but was based on similar studies in the field. For myelinating cell culture experiments, at lest three independent experiments from each genotype were analyzed. Analyses were performed while blinded to genotype. Tissues and cells stained positively for Myc-tag were regarded as mutant. Details of p value and sample size for each comparison are detailed in Figure Legends.

KEY RESOURCES TABLE

REAGENT or RESOURCE	SOURCE	IDENTIFIER
Antibodies		
Mouse anti-MAG	EMD Millipore	RRID:AB_2137847
Rabbit anti-Myc	Sigma-Aldrich	RRID:AB_439680
Mouse anti-Neurofillament SMI-311R+SMI-312R	Chemicon	RRID:AB_509991 RRID: AB_509993,
Mouse anti-CC1	Millipore	RRID:AB_2057371
Rat anti-Neurofilament H	Millipore	RRID:AB_2043446
Rat anti-MBP	Chemicon	RRID:AB_94975
Rat anti-PLP	Peles Lab	RRID:AB_2341144
Mouse anti-Cadm4	Neuromab	RRID:AB_10673109
Rabbit anti-Opalin	Peles lab	N/A
Rabbit anti-Caspr	Peles lab	N/A
Mouse anti-Gliomedin	Peles lab	N/A
Rabbit anti-B4spectrin	Rasband lab	N/A
Mouse anti Beta Tubulin	Sigma-Aldrich	RRID:AB_2288045
Cy3-conjugated Donkey anti-mouse	Jackson	RRID:AB_2340813
Cy488-conjugated Donkey anti-rabbit	Jackson	RRID:AB_2313584
DyLight 405-conjugated Donkey anti-rat	Jackson	RRID:AB_2340681
Cy5-conjugated Donkey anti-rat	Jackson	RRID:AB_2340671
Cy3-conjugated goat-anti human Fc	Jackson	RRID:AB_2337718
Mouse anti-Myc 9E10	DHSB University of Iowa	RRID:AB_2266850
Mouse anti-O4	Barres Lab	N/A
Bacterial and Virus Strains		
XL10-Gold	Stratagene	Cat #200314
Chemicals, Peptides, and Recombinant Proteins		
Poly L-lysine	Sigma-Aldrich	Cat #P-1274
Poly D-lysine	Sigma-Aldrich	Cat #P-7405
Trypsin no EDTA	Gibco	Cat #25050
B27-supplement	Gibco	Cat #17504-044
5-Fluoro-2′-deoxyuridine	Sigma-Aldrich	Cat #F-0503
Glutamax	Gibco	Cat #15140-122
Mouse nerve growth factor (NGF)	Alomone labs	Cat #N-100
Sodium Pyruvate	Gibco	Cat #11360039
Triiodothyronine (T3)	Calbiochem	Cat #64245
L-Thyroxin (T4)	Calbiochem	Cat #61205
Penicillin Streptomycin	Gibco	Cat #15070063
DMEM-Medium	Gibco	Cat #4196-039
DMEM/F12-Medium	Gibco	Cat #10565018
Leibovitz's L-15 Medium	Gibco	Cat #11415064

REAGENT or RESOURCE	SOURCE	IDENTIFIER
Horse Serum	PAA	Cat #B15-021
Forskolin	Sigma-Aldrich	Cat #F68886
N-Acetylcysteine	Sigma-Aldrich	Cat #A0737
N2 Supplement	Gibco	Cat #17502048
Doxycycline	Sigma-Aldrich	Cat #D9891
Paraformaldehyde	Electron Microscopy Sciences	Cat #15714
Cacodylate	Electron Microscopy Sciences	Cat #11650
Glutaraldehyde	Electron Microscopy Sciences	Cat #16000
Fluoromount-G	Thermo Fisher Scientific	Cat #00-4958-02
NanoAligned nanofiber	Nanofiber Solutions	Cat #121202
Hydrocortisone	Sigma-Aldrich	Cat # H-0396
Biotin	Sigma-Aldrich	Cat #B4501
Insulin	Sigma-Aldrich	Cat #I18882
Trypsin	Gibco	Cat #15090-046
Collagenase	Gibco	Cat #17100-017
Soy bean trypsin inhibitor	Sigma-Aldrich	Cat #T65222
Deoxyribonuclease I	Sigma-Aldrich	Cat #DN25
Bovine serum albumin fraction V	Sigma-Aldrich	Cat #A3059
Poly-L-ornithine solution	Sigma-Aldrich	Cat #P4957
Matrigel	Becton Dickinson	Cat #356234
Novaultra luxol fast blue stain kit	IHC-WORLD	Cat #IW-3005
Experimental Models: Cell Lines		
Phoenix-ECO		N/A
Critical Commercial Assays		
KAPA HiFi HotStart Ready MixPCR Kit	KAPA BIOSYSTEMS	Cat #KK2600 07958919001
T4 DNA Ligase	Thermo-Fisher	Cat #EL0014
Proteinase inhibitor cocktail	MILIPORE	Cat #539134-10ML
Experimental Models: Organisms/Strains		
Rat: whistler	Envigo	RGD_13525002
Mouse: C57BL/6	Golan et al., 2013	RRID:MGI:5656552
Mouse: mbp:Cadm4dCT	Golan et al., 2013	N/A
Mouse: *CADM2* knockout	Golan et al., 2013	N/A
Mouse: *CADM3* knockout	Golan et al., 2013	N/A
Mouse: S-MAG-GFP	Erb et al., 2006	N/A
CNP-Cre Rosa26-lacZfloxDTA	Brockschnieder et al., 2006	N/A
Recombinant DNA		
pMX-Tetone Cadm4dCT	This paper	N/A
pSX-FC	Spiegel et al., 2007	N/A
pSX-Cadm1FC	Spiegel et al., 2007	N/A

REAGENT or RESOURCE	SOURCE	IDENTIFIER
pSX-Cadm2FC	Spiegel et al., 2007	N/A
pSX-Cadm3FC	Spiegel et al., 2007	N/A
pSX-Cadm4FC	Spiegel et al., 2007	N/A
Software and Algorithms		
FIGI	NIH	RRID:SCR_002285
Adobe Photoshop CS5 Adobe	N/A	RRID:SCR_014199
Other		
LSM700 confocal microscope	Carl Zeiss	N/A
Pannoramic digital slide scanner	3DHISTECH	N/A
T12 transmission electron microscope	FEI	N/A
Tecnai Spirit transmission electron microscope	FEI	N/A

Supplementary Material

Refer to Web version on PubMed Central for supplementary material.

ACKNOWLEDGMENTS

We thank Veronique Amor for insightful comments. This work was supported by the NIH (R01NS097428), the Israel Science Foundation, and the Dr. Miriam and Sheldon G. Adelson Medical Research Foundation and a research grant from the Estate of Lilly Fulop. E.P. is the Incumbent of the Hanna Hertz Professorial Chair for Multiple Sclerosis and Neuroscience.

REFERENCES

Almeida RG, and Lyons DA (2014). On the resemblance of synapse formation and CNS myelination. Neuroscience 276, 98–108. [PubMed: 24035825]

Almeida RG, Pan S, Cole KLH, Williamson JM, Early JJ, Czopka T, Klingseisen A, Chan JR, and Lyons DA (2018). Myelination of neuronal cell bodies when myelin supply exceeds axonal demand. Curr Biol 28, 1296–1305 e1295. [PubMed: 29628374]

Bechler ME, Byrne L, and Ffrench-Constant C (2015). CNS Myelin Sheath Lengths Are an Intrinsic Property of Oligodendrocytes. Curr Biol 25, 2411–2416. [PubMed: 26320951]

Brockschnieder D, Sabanay H, Riethmacher D, and Peles E (2006). Ermin, a myelinating oligodendrocyte-specific protein that regulates cell morphology. The Journal of neuroscience : the official journal of the Society for Neuroscience 26, 757–762. [PubMed: 16421295]

Czopka T, Ffrench-Constant C, and Lyons DA (2013). Individual oligodendrocytes have only a few hours in which to generate new myelin sheaths in vivo. Dev Cell 25, 599–609. [PubMed: 23806617]

Erb M, Flueck B, Kern F, Erne B, Steck AJ, and Schaeren-Wiemers N (2006). Unraveling the differential expression of the two isoforms of myelin-associated glycoprotein in a mouse expressing GFP-tagged S-MAG specifically regulated and targeted into the different myelin compartments. Mol Cell Neurosci 31, 613–627. [PubMed: 16442810]

Fogel AI, Li Y, Giza J, Wang Q, Lam TT, Modis Y, and Biederer T (2010). N-glycosylation at the SynCAM (synaptic cell adhesion molecule) immunoglobulin interface modulates synaptic adhesion. J Biol Chem 285, 34864–34874. [PubMed: 20739279]

Fowler DK, Peters JH, Williams C, and Washbourne P (2017). Redundant Postsynaptic Functions of SynCAMs 1-3 during Synapse Formation. Front Mol Neurosci 10, 24. [PubMed: 28197078]

Galuska SP, Rollenhagen M, Kaup M, Eggers K, Oltmann-Norden I, Schiff M, Hartmann M, Weinhold B, Hildebrandt H, Geyer R, et al. (2010). Synaptic cell adhesion molecule SynCAM 1 is a target for

polysialylation in postnatal mouse brain. Proc Natl Acad Sci U S A 107, 10250–10255. [PubMed: 20479255]

Golan N, Adamsky K, Kartvelishvily E, Brockschnieder D, Mobius W, Spiegel I, Roth AD, Thomson CE, Rechavi G, and Peles E (2008). Identification of Tmem10/Opalin as an oligodendrocyte enriched gene using expression profiling combined with genetic cell ablation. Glia 56, 1176–1186. [PubMed: 18571792]

Golan N, Kartvelishvily E, Spiegel I, Salomon D, Sabanay H, Rechav K, Vainshtein A, Frechter S, Maik-Rachline G, Eshed-Eisenbach Y, et al. (2013). Genetic deletion of Cadm4 results in myelin abnormalities resembling Charcot-Marie-Tooth neuropathy. The Journal of neuroscience : the official journal of the Society for Neuroscience 33, 10950–10961. [PubMed: 23825401]

Hines JH, Ravanelli AM, Schwindt R, Scott EK, and Appel B (2015). Neuronal activity biases axon selection for myelination in vivo. Nat Neurosci 18, 683–689. [PubMed: 25849987]

Lee S, Leach MK, Redmond SA, Chong SY, Mellon SH, Tuck SJ, Feng ZQ, Corey JM, and Chan JR (2012). A culture system to study oligodendrocyte myelination processes using engineered nanofibers. Nature methods 9, 917–922. [PubMed: 22796663]

Marques S, Zeisel A, Codeluppi S, van Bruggen D, Mendanha Falcao A, Xiao L, Li H, Haring M, Hochgerner H, Romanov RA, et al. (2016). Oligodendrocyte heterogeneity in the mouse juvenile and adult central nervous system. Science 352, 1326–1329. [PubMed: 27284195]

Maurel P, Einheber S, Galinska J, Thaker P, Lam I, Rubin MB, Scherer SS, Murakami Y, Gutmann DH, and Salzer JL (2007). Nectin-like proteins mediate axon Schwann cell interactions along the internode and are essential for myelination. J Cell Biol 178, 861–874. [PubMed: 17724124]

Osso LA, and Chan JR (2017). Architecting the myelin landscape. Curr Opin Neurobiol 47, 1–7. [PubMed: 28709021]

Park J, Liu B, Chen T, Li H, Hu X, Gao J, Zhu Y, Zhu Q, Qiang B, Yuan J, et al. (2008). Disruption of Nectin-like 1 cell adhesion molecule leads to delayed axonal myelination in the CNS. The Journal of neuroscience : the official journal of the Society for Neuroscience 28, 12815–12819. [PubMed: 19036974]

Redmond SA, Mei F, Eshed-Eisenbach Y, Osso LA, Leshkowitz D, Shen YA, Kay JN, Aurrand-Lions M, Lyons DA, Peles E, et al. (2016). Somatodendritic Expression of JAM2 Inhibits Oligodendrocyte Myelination. Neuron 91, 824–836. [PubMed: 27499083]

Sharma K, Schmitt S, Bergner CG, Tyanova S, Kannaiyan N, Manrique-Hoyos N, Kongi K, Cantuti L, Hanisch UK, Philips MA, et al. (2015). Cell type- and brain region-resolved mouse brain proteome. Nat Neurosci 18, 1819–1831. [PubMed: 26523646]

Snaidero N, Mobius W, Czopka T, Hekking LH, Mathisen C, Verkleij D, Goebbels S, Edgar J, Merkler D, Lyons DA, et al. (2014). Myelin membrane wrapping of CNS axons by PI(3,4,5)P3-dependent polarized growth at the inner tongue. Cell 156, 277–290. [PubMed: 24439382]

Snaidero N, and Simons M (2017). The logistics of myelin biogenesis in the central nervous system. Glia 65, 1021–1031. [PubMed: 28168748]

Spiegel I, Adamsky K, Eshed Y, Milo R, Sabanay H, Sarig-Nadir O, Horresh I, Scherer SS, Rasband MN, and Peles E (2007). A central role for Necl4 (SynCAM4) in Schwann cell-axon interaction and myelination. Nat Neurosci 10, 861–869. [PubMed: 17558405]

Takai Y, Miyoshi J, Ikeda W, and Ogita H (2008). Nectins and nectin-like molecules: roles in contact inhibition of cell movement and proliferation. Nat Rev Mol Cell Biol 9, 603–615. [PubMed: 18648374]

Tanabe Y, Kasahara T, Momoi T, and Fujita E (2008). Neuronal RA175/SynCAM1 isoforms are processed by tumor necrosis factor-alpha-converting enzyme (TACE)/ADAM17-like proteases. Neurosci Lett 444, 16–21. [PubMed: 18718504]

Watkins TA, Emery B, Mulinyawe S, and Barres BA (2008). Distinct stages of myelination regulated by gamma-secretase and astrocytes in a rapidly myelinating CNS coculture system. Neuron 60, 555–569. [PubMed: 19038214]

Yang ML, Shin J, Kearns CA, Langworthy MM, Snell H, Walker MB, and Appel B (2015). CNS myelination requires cytoplasmic dynein function. Dev Dyn 244, 134–145. [PubMed: 25488883]

Zhang Y, Chen K, Sloan SA, Bennett ML, Scholze AR, O'Keeffe S, Phatnani HP, Guarnieri P, Caneda C, Ruderisch N, et al. (2014). An RNA-sequencing transcriptome and splicing database of glia,

neurons, and vascular cells of the cerebral cortex. The Journal of neuroscience : the official journal of the Society for Neuroscience 34, 11929–11947. [PubMed: 25186741]

Zhu Y, Li H, Li K, Zhao X, An T, Hu X, Park J, Huang H, Bin Y, Qiang B, et al. (2013). Necl-4/SynCAM-4 is expressed in myelinating oligodendrocytes but not required for axonal myelination. PLoS One 8, e64264. [PubMed: 23700466]

Highlights

- Increase expression of Cadm4 in oligodendrocytes inhibits myelination.
- Axoglial interaction mediated by Cadm proteins regulate myelin targeting.
- Myelination requires tightly regulated axoglial adhesion.

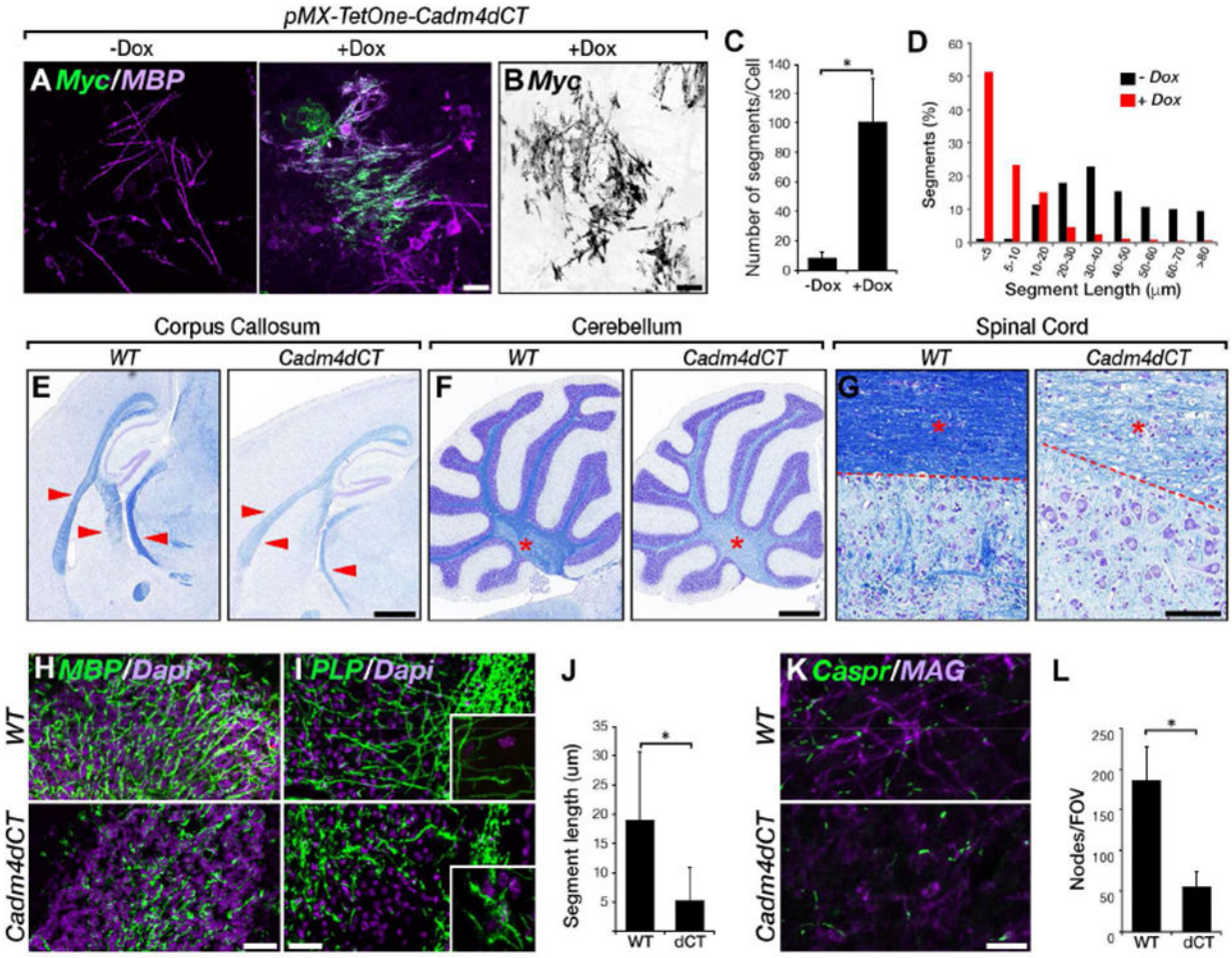

Figure 1. Expression of the extracellular domain of Cadm4 in oligodendrocytes interferes with myelination.

A-B. Cadm4dCT forms short cellular processes that fail to myelinate. Rat OPCs infected with a viral vector containing myc-tagged Cadm4dCT under a tetracycline inducible promoter were treated with Doxycycline (Dox) as indicated, and immunolabeled with antibodies to Myc and MBP. Note the abnormal morphology of anti-Myc labeled oligodendrocyte as shown in B as a color-inverted image. Treatment of uninfected cultures with Doxycycline had no effect (data not shown). **C-D.** Quantitation of the number of MBP-positive segments produced by a single oligodendrocyte (C) and segment length distribution (D) of retroviral infected OLs treated with doxycycline as indicated (±Dox). Bars represent average ± STDV of 14-20 cells isolated from three independent experiments. **E-G.** Transgenic mice expressing Cadm4dCT are hypomyelinated. Sagittal sections of brains containing corpus callosum (E), cerebellum (F), and of spinal cord (G) isolated from wild type *(WT)* and *Cadm4dCT* transgenic mice, stained with Luxol Fast Blue (LFB) and hematoxylin and eosin. Hypomyelination is detected in the corpus callosum, fimbria and the fornix (E; arrowheads), as well as in the cerebellum and the spinal cord (F-G; asterisk). A dashed line marks the border between the white and gray matter in the spinal cord. **H-I.**

Sagittal section of the cerebellum (E) and piriform cortex (F) isolated from the indicated genotypes, immunolabeled with antibodies to MBP (H) and PLP (I). Dapi was used to stain the nuclei. **J.** *Cadm4dCT* exhibits shorter myelin segments. Segment length was measured from PLP-labeled cortices of wild type (WT) and *Cadm4dCT* transgenic mice (dCT). Bars represent average ± STDV of 4-5 wide-scale panoramic image fields counted from three mice of each genotype (*p<0.005, Student's t-test). **K.** Cortical sections from the indicated genotypes immunolabeled using antibodies to Caspr and MAG. **L.** Quantitation of the number of nodes per field of view (FOV; cortical layers 2-5) identified by the presence of flanking Caspr-positive paranodal junctions. Bars represent average ± STDV of 12 fields counted from three mice of each genotype (*p<0.005, Student's t-test). Scale bars: A-B, 20 mm; E and G, 500 μm; F, 100 μm; H-I and K, 10 μm. See also Figure S1.

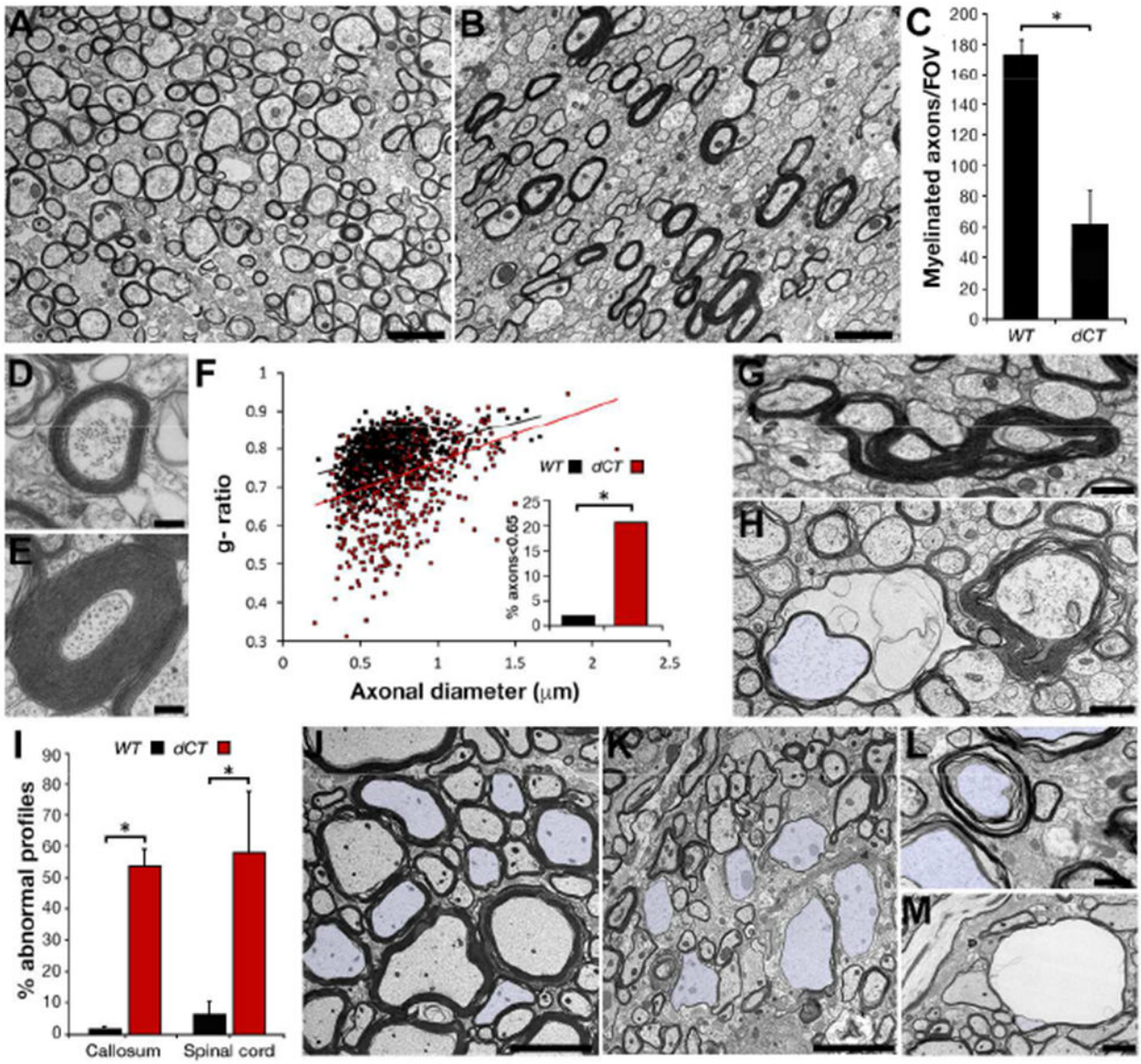

Figure 2. *Cadm4dCT transgenic* mice exhibit multiple myelin abnormalities.

A-B. Electron micrographs of midsagittal sections of the corpus callosum from 3-months-old wild type (A) and *Cadm4dCT* (B) mice. **C.** Number of myelinated axons per field of view (FOV). Bars represent mean ± SEM of at least 1000 axons counted from three mice of each genotype (*p<0.005, Student's t-test). **D-E.** Higher magnification images of myelinated axons from wild type (D) and *Cadm4dCT* transgenic mice (E). **F.** g-ratio as a function of axonal diameter. *Cadm4dCT* show lower g-ratio than wild type. Total of at least 600 axons from 3 mice of each genotype were analyzed. Inset shows the percentage of axons displaying g-ratio smaller than 0.65. **G-H.** *Cadm4dCT* corpus callosum exhibits myelin outfolds (G), and the formation of myelin splitting and vacuolization (H). **I.** *Cadm4dCT* mice exhibit a substantial number of myelin abnormalities. Percentage of abnormal myelin

profiles detected in the corpus callosum and spinal cord from the indicated genotypes. Bars represent mean ± SEM of total of at least 1300 axons counted from three mice of each genotype (*p<0.005, Student's t-test). **J-K.** Electron micrographs showing cross sections of the spinal cord of 3-months-old wild type (J) and *Cadm4dCT* (K) mice. Note the presence of large axons that are not myelinated in the transgene (colored in K). **L-M.** Higher magnification images of *Cadm4dCT* spinal cord showing myelin splitting (L) and presence of a large vacuole (M). Scale bars, A-B, 2 μm; D-E, 0.2 μm; G-H, L-M 1 μm; J-K, 0.5 μm.

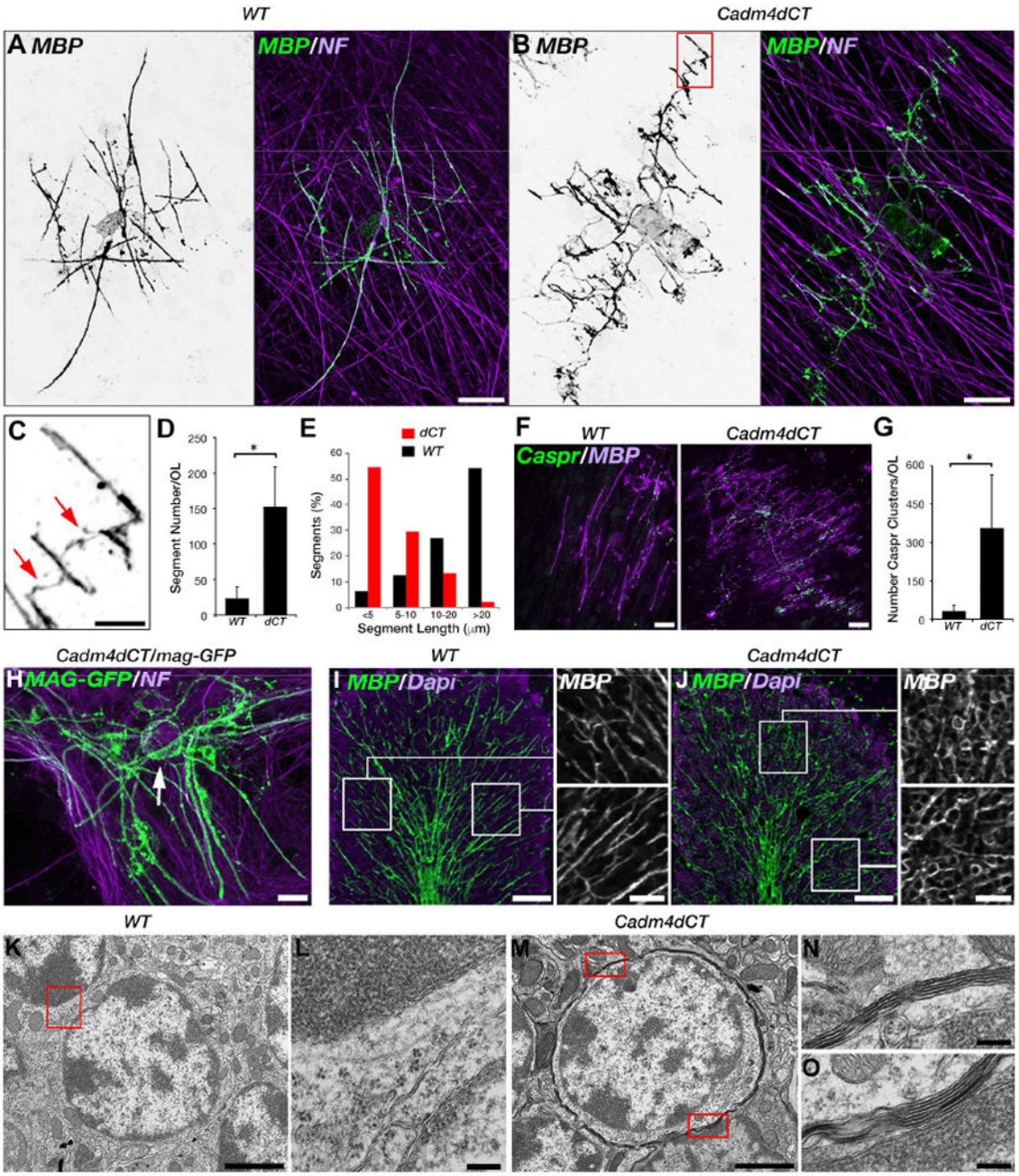

Figure 3. *Cadm4dCT* oligodendrocytes produced numerous contact sites but failed to elongate and generate mature myelin internodes.

A. Single cell analysis of myelinating OLs using antibodies to MBP and neurofilament (NF). Myelinating OPCs/DRG neurons cultures were prepared using OPCs isolated from wild type (A) and *Cadm4dCT* (B) mice. The MBP channel is also shown on the left of each panel as a color-inverted image. **C.** Higher magnification of the boxed area in B. Note the cellular extensions (arrowheads) linking short immature myelin segments that are present on different axons. **D-E.** Quantitation of the number (D) and length distribution (E) of MBP-

positive segments produced by a single oligodendrocyte from each genotype. Bars represent average ± STDV of 7-10 cells isolated from three mice of each genotype (*p<0.005, Student's t-test). **F.** Myelinating culture using OPCs isolated from wild type *(WT)* and *Cadm4dCT* mice immunolabeled with antibodies to Caspr and MBP. Note the numerous Caspr clusters elicited by a single *Cadm4dCT* oligodendrocyte. **G.** Quantitation of the number of Caspr clusters associated with individual OLs. Bars represent average ± STDV of 12 cells analyzed from each genotype (*p<0.005, Student's t-test). **H-O.** *Cadm4dCT* OLs ensheath and myelinate neuronal cell bodies. **H.** Myelinating spinal cord culture prepared from a double *Cadm4dCT* and *MAG-GFP* transgenic showing the ensheathment of MAG-positive processes around a cell body (arrow). **I-J.** Longitudinal sections of the cerebellum prepared from wild type (I) and *Cadm4dCT* (J) mice were labeled for MBP. Dapi was used to stain the nuclei. Higher magnification of the anti-MBP labeling in the boxed areas is shown on the right. **K-O.** Electron micrographs of sagittal sections of the cerebellum of 3-months-old wild type (K-L) and *Cadm4dCT* (M-O) mice. Higher magnification of the boxed areas in K and M is shown in L, and N-O, respectively. Note the presence of multiple myelin layers around the cell body (N-O). Scale bars, A-B, 20 μm; C and F, 5 μm; H, 20 μm; I-J, 50 μm and insets 20 μm; K, M, 2 μm; L, N-O, 0.2 μm. See also Figure S3.

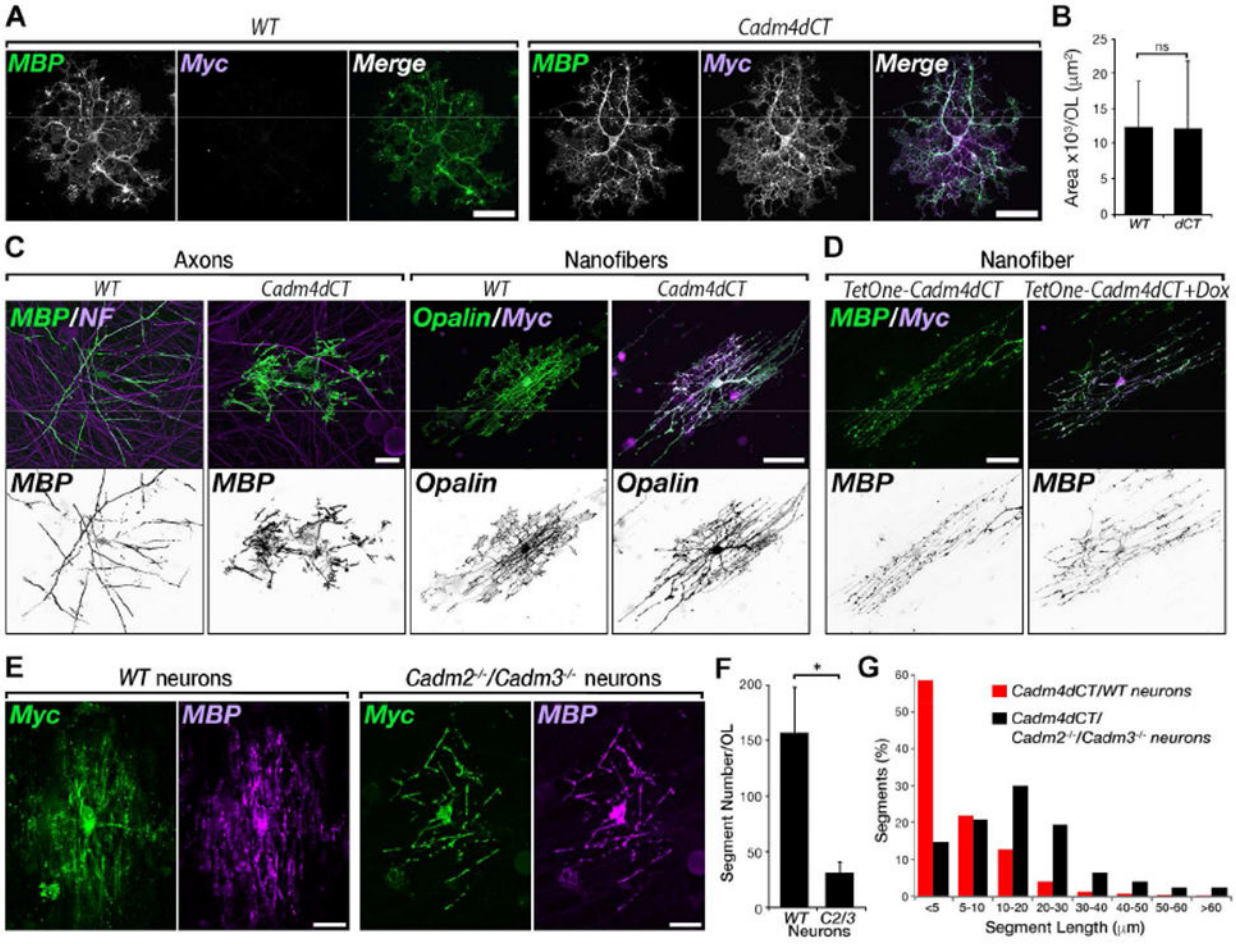

Figure 4. Cadm4dCT OLs phenotype results from aberrant neuron-glia adhesion.

A. *Cadm4dCT* OLs look similar to wild type cells when cultured in the absence of neurons. Wild type *(WT)* and Cadm4dCT OPC cultures were immunolabeled with antibodies to Myc and MBP. **B.** Wild type and *Cadm4dCT* display a similar oligodendrocyte MBP-positive area. Bars represent average ± STDV of 15-20 cells isolated from three mice of each genotype (n.s, non-significance). **C.** OPCs isolated from wild type *(WT)* or *Cadm4dCT* mice were grown on DRG neurons or nanofibers. Cultures were fixed and immunolabeled with antibodies to MBP and neurofilament or to Opalin and Myc as indicated. The corresponding single MBP and Opalin channels are also shown below each panel as a color-inverted image. **D.** Rat OPCs infected with a viral vector containing myc-tagged Cadm4dCT under a tetracycline inducible promoter were left untreated *(TetOne-Cadm4dCT)* or treated with Doxycycline *(TetOne-Cadm4dCT+Dox)* and grown on nanofibers. Slides were fixed and immunolabeled with antibodies to Myc and MBP. MBP immunoreactivity is shown below each panel as a color-inverted image. **E.** Culture of *Cadm4dCT* OLs on DRG neurons lacking its axonal receptors diminishes the morphological abnormality. *Cadm4dCT* OPCs were cultured with DRG neurons isolated from wild type *(WT)* mice, or mice lacking both Cadm2 and Cadm3 (*Cadm2*$^{-/-}$/*Cadm3*$^{-/-}$). Immunolabeling was carried out using antibodies

to Myc and MBP. F. Quantitation showing that *Cadm4dCT* OPCs cultured on *Cadm2*$^{-/-}$/*Cadm3*$^{-/-}$ neurons (C2/3) exhibit fewer myelin segments compared to cells cultured on wild type neurons. Bars represent average ± STDV of 10-13 cells analyzed from each condition (*p<0.005, Student's t-test). **G.** Segment length distribution analysis of Cadm4dCT OPCs cultured on wild type or *Cadm2*$^{-/-}$/*Cadm3*$^{-/-}$ neurons. Scale bars, A, D, 50 μm; C, E, 20 μm. See also Figure S4.

REAGENT or RESOURCE	SOURCE	IDENTIFIER
Antibodies		
Mouse anti-MAG	EMD Millipore	RRID:AB_2137847
Rabbit anti-Myc	Sigma-Aldrich	RRID:AB_439680
Mouse anti-Neurofillament SMI-311R+SMI-312R	Chemicon	RRID:AB_509991 RRID: AB_509993,
Mouse anti-CC1	Millipore	RRID:AB_2057371
Rat anti-Neurofilament H	Millipore	RRID:AB_2043446
Rat anti-MBP	Chemicon	RRID:AB_94975
Rat anti-PLP	Peles Lab	RRID:AB_2341144
Mouse anti-Cadm4	Neuromab	RRID:AB_10673109
Rabbit anti-Opalin	Peles lab	N/A
Rabbit anti-Caspr	Peles lab	N/A
Mouse anti-Gliomedin	Peles lab	N/A
Rabbit anti-B4spectrin	Rasband lab	N/A
Mouse anti Beta Tubulin	Sigma-Aldrich	RRID:AB_2288045
Cy3-conjugated Donkey anti-mouse	Jackson	RRID:AB_2340813
Cy488-conjugated Donkey anti-rabbit	Jackson	RRID:AB_2313584
DyLight 405-conjugated Donkey anti-rat	Jackson	RRID:AB_2340681
Cy5-conjugated Donkey anti-rat	Jackson	RRID:AB_2340671
Cy3-conjugated goat-anti human Fc	Jackson	RRID:AB_2337718
Mouse anti-Myc 9E10	DHSB University of Iowa	RRID:AB_2266850
Mouse anti-O4	Barres Lab	N/A
Bacterial and Virus Strains		
XL10-Gold	Stratagene	Cat #200314
Chemicals, Peptides, and Recombinant Proteins		
Poly L-lysine	Sigma-Aldrich	Cat #P-1274
Poly D-lysine	Sigma-Aldrich	Cat #P-7405
Trypsin no EDTA	Gibco	Cat #25050
B27-supplement	Gibco	Cat #17504-044
5-Fluoro-2′-deoxyuridine	Sigma-Aldrich	Cat #F-0503
Glutamax	Gibco	Cat #15140-122
Mouse nerve growth factor (NGF)	Alomone labs	Cat #N-100
Sodium Pyruvate	Gibco	Cat #11360039
Triiodothyronine (T3)	Calbiochem	Cat #64245
L-Thyroxin (T4)	Calbiochem	Cat #61205
Penicillin Streptomycin	Gibco	Cat #15070063
DMEM-Medium	Gibco	Cat #4196-039
DMEM/F12-Medium	Gibco	Cat #10565018
Leibovitz's L-15 Medium	Gibco	Cat #11415064

REAGENT or RESOURCE	SOURCE	IDENTIFIER
Horse Serum	PAA	Cat #B15-021
Forskolin	Sigma-Aldrich	Cat #F68886
N-Acetylcysteine	Sigma-Aldrich	Cat #A0737
N2 Supplement	Gibco	Cat #17502048
Doxycycline	Sigma-Aldrich	Cat #D9891
Paraformaldehyde	Electron Microscopy Sciences	Cat #15714
Cacodylate	Electron Microscopy Sciences	Cat #11650
Glutaraldehyde	Electron Microscopy Sciences	Cat #16000
Fluoromount-G	Thermo Fisher Scientific	Cat #00-4958-02
NanoAligned nanofiber	Nanofiber Solutions	Cat #121202
Hydrocortisone	Sigma-Aldrich	Cat # H-0396
Biotin	Sigma-Aldrich	Cat #B4501
Insulin	Sigma-Aldrich	Cat #I18882
Trypsin	Gibco	Cat #15090-046
Collagenase	Gibco	Cat #17100-017
Soy bean trypsin inhibitor	Sigma-Aldrich	Cat #T65222
Deoxyribonuclease I	Sigma-Aldrich	Cat #DN25
Bovine serum albumin fraction V	Sigma-Aldrich	Cat #A3059
Poly-L-ornithine solution	Sigma-Aldrich	Cat #P4957
Matrigel	Becton Dickinson	Cat #356234
Novaultra luxol fast blue stain kit	IHC-WORLD	Cat #IW-3005
Experimental Models: Cell Lines		
Phoenix-ECO		N/A
Critical Commercial Assays		
KAPA HiFi HotStart Ready MixPCR Kit	KAPA BIOSYSTEMS	Cat #KK2600 07958919001
T4 DNA Ligase	Thermo-Fisher	Cat #EL0014
Proteinase inhibitor cocktail	MILIPORE	Cat #539134-10ML
Experimental Models: Organisms/Strains		
Rat: whistler	Envigo	RGD_13525002
Mouse: C57BL/6	Golan et al., 2013	RRID:MGI:5656552
Mouse: mbp:Cadm4dCT	Golan et al., 2013	N/A
Mouse: *CADM2* knockout	Golan et al., 2013	N/A
Mouse: *CADM3* knockout	Golan et al., 2013	N/A
Mouse: S-MAG-GFP	Erb et al., 2006	N/A
CNP-Cre Rosa26-lacZfloxDTA	Brockschnieder et al., 2006	N/A
Recombinant DNA		
pMX-Tetone Cadm4dCT	This paper	N/A
pSX-FC	Spiegel et al., 2007	N/A
pSX-Cadm1FC	Spiegel et al., 2007	N/A

REAGENT or RESOURCE	SOURCE	IDENTIFIER
pSX-Cadm2FC	Spiegel et al., 2007	N/A
pSX-Cadm3FC	Spiegel et al., 2007	N/A
pSX-Cadm4FC	Spiegel et al., 2007	N/A
Software and Algorithms		
FIGI	NIH	RRID:SCR_002285
Adobe Photoshop CS5 Adobe	N/A	RRID:SCR_014199
Other		
LSM700 confocal microscope	Carl Zeiss	N/A
Pannoramic digital slide scanner	3DHISTECH	N/A
T12 transmission electron microscope	FEI	N/A
Tecnai Spirit transmission electron microscope	FEI	N/A